IAEA Technical Committee Meeting on
*"Evaluation of Material Coolant Interaction and Material Movement and Relocation in Liquid Metal Fast Reactors"*

# FUEL PIN BEHAVIOUR UNDER CONDITIONS OF CONTROL ROD WITHDRAWAL ACCIDENT IN CABRI-2 EXPERIMENTS

Joëlle PAPIN
Francette LEMOINE
Institut de Protection et de Sûreté Nucléaire
IPSN/CEA
13108 St. Paul lez Durance
FRANCE

Ikken SATO
PNC
4002 Narita-machi, 0-arai machi
Ibaraki-ken, 311-13
JAPON

Dankward STRUWE
Werner PFRANG
Institut fur Reaktorsicherheit
Kernforschungszentrum
D 76021 Karlsruhe
GERMANY

## ABSTRACT

Simulation of the control rod withdrawal accident has been performed in the international CABRI-2 experimental programme. The tests realized with industrial pins led to clarify the influence of the pellet design and have shown the important role of fission products on the solid fuel swelling which promotes early pin failure with solid fuel pellet. With annular pellet design, large fuel swelling combined to low smear density leads to degradation of fuel thermal conductivity and thus reduces power to melt. However, the high margin to deterministic failure is confirmed with hollow pellets. Improvements of the modelling were necessary to describe such behaviours in computer codes as SAS-4A, PAPAS-2S and PHYSURAC.

## I. INTRODUCTION

In the CABRI-2 international experimental programme realized under IPSN, KFK and PNC collaboration [1], simulation of the control rod withdrawal accident has been performed using industrial irradiated pins submitted to a slow power ramp of around 1 % PN/s starting from nominal conditions.

The main questions rising in the frame of this design basis accident concern :

- the knowledge of the power to melt resulting from fuel thermal evolution and related fissions gases behaviour,
- the evaluation of the margin existing between the power level of emergency reactor scram and the power corresponding to a deterministic pin failure,
- the determination of the risk of molten fuel ejection from an adventitious pin failure with molten volume fraction of 10 to 20 % and the potential for pin to pin propagation inside a subassembly.

Indeed, the conditions of such slow transients in which the fuel pin and the coolant are almost in thermal equilibrium, are different from those already investigated in the other CABRI experiments [2], [3], and specific pin behaviour might be expected. One important point is the kinetics of fission gases release in solid and liquid fuel which influences the answer to the three previous questions by the way of fuel swelling, pressurisation of the molten fuel cavity and in pin fuel motion inside the available free volume (case of an annular pin design).

Three tests have been realized using different pin designs : solid pellets at 12 at % burn-up (E12 test with Viggen-4 pin) and annular pellets at 5 at % burn-up (E9 and E9bis tests with Ophelie-6 pins).

The main objectives of the tests E9 and E12 were to investigate the fuel pin behaviour in such conditions, to evaluate the margin to failure of those pins, and to determine the influence of both pellet designs on these points (in spite of the different irradiation levels of the pins).

A particular objective in support of the Super-Phenix 1 (SPX1) reactor studies, has been assigned to the test E9bis which was to study the risk of molten fuel ejection in case of the adventitious failure of an annular pin similar to SPX1 ones, having 20 % of molten fuel in mass. In order to initiate failure in those conditions, the clad has been weakened by a notch located at peak power node.

In this paper, we present the experimental results and their interpretation together with quantitative evaluation based on theoretical modelling. The models used are SAS-4A (KFK), PAPAS-2S (PNC) and PHYSURAC (CEA). Finally, the main outcomes for the study of control rod withdrawal accident are summarized.

## II. THE CABRI-2 SLOW POWER TESTS

### II.1. Test Pins characteristics

Both types of pins used in these tests are composed of mixed oxide fuel and have been irradiated in the fast breeder PHENIX reactor.

Their main characteristics are summarized in the following table 1 :

| TEST PIN | | OPHELIE-6 | VIGGEN-4 |
|---|---|---|---|
| Fuel design | | hollow | solid |
| Pellet outer diameter * | (mm) | 7.27 | 5.427 |
| Pellet inner diameter * | (mm) | 2. | -- |
| Fissile length | (mm) | 750 | 850 |
| Maximum burn-up | (at %) | 4.9 | 11.7 |
| End of life peak linear power | (W/cm) | 305 | 310 |
| Clad material : stainless steel | | 316 cold work | 15.15 Ti, cold work |
| Clad outer diameter * | (mm) | 8.65 | 6.55 |
| Clad inner diameter * | (mm) | 7.50 | 5.65 |
| dpa NRT max | | 58 | 98 |
| Fuel smear density after irradiation | | 80 % | 91 % |
| Plenum pressure at 400°C | (MPa) | 1.2 | 5.7 |

* as fabricated value

Although the mean gas retention at peak power node is similar in both pins (around 400 $mm^3/g$ STP) the radial profile in Viggen-4 pins is much more pronounced with no retention in the center and high value in the outer zone of the pellets.

One important point to understand the test results is the difference of fuel smear density in both pins.
In the Viggen-4 pins, in spite of high burn-up level, small cladding swelling (1 %) has been obtained after irradiation campaign : this leads to a narrow fuel-clad gap which promotes PCMI (pellet-clad mechanical interaction) during power transients. However clad mechanical tests from the Viggen-4 pins showed that sufficient ductility still exists which balances the PCMI loading with regards to failure threshold.
In the Ophelie-6 pins, the already low smear density with hollow pellet design is reduced by large clad swelling due to cladding material at 5 at % burn-up level : this mitigates the PCMI effects during power transients.

On the other hand, examinations of the fuel outer region of the Viggen-4 fuel presents significant grain fragmentation with small grain size (~ 1 μm) and micro-porosity increase with large gas bubbles at the grain boundary.

The following other features characterize the highly irradiated Viggen-4 pins :

- the presence of clad corrosion layer in the upper part of the pins which might influence the PCMI by the reduction of the fuel to clad gap at these levels ; however, no significant corrosion has been measured in the pin used for the E12 test,
- the presence of gap compounds (called "JOG") which most probably modify the gap conditions during the pre-irradiation ; however, under strong PCMI and hot conditions gap compound layer is expected to decrease,
- the presence of volatile fission products as Cs, the vaporisation of which during transient might contribute to fuel swelling.

## II.2. The slow power ramp tests conditions

The test pins are located in an annular test section inside the sodium loop of the CABRI reactor (75 cm fissile height).
The slow power ramps are initiated from CABRI steady-state conditions. The table 2 gives the main characteristics of the transients :

| | E9 | E9bis | E12 |
|---|---|---|---|
| Initial maximum linear power Po (W/cm) | 603 | 594 | 474 |
| Power ramp (% Po/s) | 1.1 | 0.95 | 0.9 |
| Final maximum linear power (W/cm) | 1347 | 1075 | 810 |
| Radial power depression in CABRI ($P_{min}/P_{max}$) | 0.45 | 0.45 | 0.3 |
| Initial sodium heat-up along fissile length from 400°C (°C) | 180 | 180 | 216 |

In E9bis test, designed with a notch at PPN (peak power node) in order to promote failure, the maximum power of 1075 W/cm has been maintained during 166 s and then a loss of flow of 40 % during 26 s has been performed followed by scram onset.

In both tests, E9 and E9bis, the pin did not fail : although this was expected in E9, the absence of failure in E9bis has been explained by the non-ideal shape of the notch (no sharp V) leading to reduction of stress concentration and the conservatism of the mechanical properties used for failure prediction.

In the E12 test, pin failure has been detected at 60 cm/BFC (bottom of fissile length) when the maximum linear power reached 810 W/cm. It was followed by an automatically initiated scram, 150 ms later, thus freezing pin conditions at the failure time.

## II.3. E9 and E9bis tests analysis

The results of these two tests are very consistent and are gained through the analysis of the hodoscope signals and the non-destructive and destructive post-test examinations.

## II.3.1. Fuel thermal behaviour

The hodoscope signals analysis showed without any doubt and with good statistics that early fuel losses occurred locally from maximum linear power of 730 W/cm (see fig. 1). According to the hodoscope conversion curve these negative variations correspond to losses of 30 % to 40 % of the initial mass for respective local powers of 755 W/cm and 784 W/cm.

The fact that fuel losses are seen without association of positive signals corresponding to the mass displaced is due to the sensitivity of the hodoscope which is higher for losses than gains related to self-shielding effect.

Later in the power transient, upwards propagation of fuel losses have been detected with maximum power beyond 900 W/cm and are clearly related to fuel melting with bubbles forming a gas blanket at the top of the melt cavity.
The final melting extension roughly follows the axial power profile and is summarized in table 3 :

| | | E9 | E9bis |
|---|---|---|---|
| Axial melt limits (mm/BFC) | upper | 690 | 635 |
| | lower | 16 | 95 |
| | axial level (mm/BFC) | | |
| Radial melt limits | 180 | 79.8 ± 1.7 | |
| (% of the external fuel radius) | 370 | 86.2 ± 1.81 | 82 ± 2 |
| | 590 | 75 ± 1.6 | |
| | 655 | 61.5 ± 0.86 | |
| Pin averaged massic melt fraction (%) | | 57 | 40 -50 |

These results clearly evidence a large fuel melting extension which, together with the early fuel mobility, indicate that fuel temperatures in those slow ramp tests with Ophelie-6 pins, have been higher than expected by code modelling at the time of the experiments (power to melt of 850 W/cm originally predicted).

Uncertainty on melting temperature versus irradiation level and on the radial power depression (± 5 %) linked to the CABRI neutronic flux could not explain such a behaviour.

The early fuel mobility could be caused by fuel sputtering of still solid fragments falling down in the central hole at the approach of fuel melting due to large temperature gradient and thermal stresses within the porous fuel zone.

The radial melting extension could be accelerated by radial relocation of the superheated liquid from the cavity towards the porous zone.

Although sputtering does hardly occur within fuel in the temperature range of 2000°C (temperature level of the porous zone), it seems difficult to allocate the E9 and E9bis tests fuel thermal behaviour to this effect with plastic fuel beyond 2500°C (at this temperature, fragments are agglomerated). Another point is the difficulty to understand the break-up in little regular fragments falling down into the central hole of 1.9 mm diameter without being rapidly stopped in place.

So, from this analysis it is more reasonable to interpret the first phenomena observed by the hodoscope around the maximum power level of 730 W/cm as the consequence of early fuel melting.

The detailed analysis of the hodoscope signals rather show the formation of several zones with gases trapped inside the liquid fuel for a long time due to reduction of the central hole diameter and possible closure even before melting onset.

On the other hand, radial cuts of E9 and E9bis at PPN show loss of density and fuel fragmentation in the unmolten zones which can be understood as a consequence of an important solid fuel swelling due to fission gases and porosity gases.

So, from this analysis it comes out that such a low power to melt together with large final melting extension can be explained consistently by large solid fuel swelling during the slow heat-up with central hole reduction which leads to the decrease of the fuel density and thus to the degradation of the thermal conductivity contributing to temperature increase.

In the annular Ophelie-6 pins, this phenomenon is probably favoured by the low smear density (80 % after irradiation campaign).

The heat-up to the CABRI steady-state at a peak linear rating of 600 W/cm higher than the end of life conditions (375 W/cm in CABRI) has also partly contributed to increase the fuel swelling because of the faster kinetics of power rising compared to operating conditions (competition between swelling and gas escape to the plenum).

### II.3.2. In pin fuel motion

The neutron - radiographies and the axial cuts revealed the occurrence of in pin fuel motion in E9 and E9bis.

In the lower parts, it is nevertheless difficult to distinguish between fuel squirting and progression of the melt cavity which reached low levels near BFC.
In the upper parts, there is a clear evidence of the central hole filled with liquid fuel up to the top of the fissile column where upwards penetration is stopped by the solid fertile pellets.

On the other hand, the absence of accumulation of metallic fission products at the top of the fissile length in spite of liquid fuel relocation at this level, indicates that the duration of the motion has been slow enough to allow segregation of these products from liquid fuel (more than 1s).

This process is different from that of fast transients as in CABRI-1 and even in CABRI-2 E5 test (pure TOP with Ophelie-6 pin) where dragging (entrainment) of metallic fission products occurred within few 0.1 s.

Local perturbations of the linear power due to this in-pin motion has certainly occurred and has been estimated to a 5 % power increase.

Near the bottom of the fissile column in E9 and E9bis, this phenomenon has influenced the axial extension of melting but in the upper part and elsewhere in the cavity, such power increase has been negligible compared to perturbations due to bubbles progression and metallic fission products accumulation in the liquid fuel.

In addition, it is highly probable that natural convection of the liquid fuel has also occurred. However, due to the evidence of several bubbles along the pin, the existence of a single loop is excluded (the melting profile would also have been affected). On the other hand, little loops of convecting liquid fuel is possible but not assured.

### II.3.3. Clad deformation and axial fuel expansion

In both tests E9 and E9bis, no extra deformation has been measured by the profilometries which shows that no significant PCMI occurred during those transients.

The axial fuel elongation given by the hodoscope is low and reversible. The value of 3 mm in E9 corresponds to clad thermal expansion and confirm that clad loading stayed below yielding with a closed gap situation.

In E9 bis, a fuel elongation of 2 mm is obtained at 65 s, which is consistent with the E9 result at the same time. After that, fuel squirting in the upper part of the fissile length prevents from the determination of fuel elongation.

Anyway, in both tests, the important in-pin motion, the gas escape to plenum and the low smear density of these pins have also most probably contribute to decrease the clad loading by the reduction of the cavity pressure.

### II.3.4. Fission gases behaviour

The measurement of gas release after pin piercing amounted to quantities of Xe and Kr respectively of 208 $cm^3$ STP in E9 and 197 $cm^3$ STP in E9bis which correspond to 28 % and 26 % of gas release due to the transient itself in both tests (71 $cm^3$ STP in E9 and 68 $cm^3$ STP in E9bis).

The close values in both tests, despite the different melting extensions indicate that the transient release comes in majority from the solid fuel.

This is confirmed by the micro-probe results which showed mainly in E9bis a decrease of the Xe concentration in the unmelted rim, proof of a strong release in this outer solid zone.

Concerning the volatile fission products, the gamma-scanning showed no axial migration of cesium. The EPMA results in E9 (at 180 and 370 mm) and in E9bis showed radial migration of the cesium to the unmelted rim and no more cesium in the molten cavity which is an indication that cesium has not contributed to molten cavity pressurisation.

## II.4. E12 test analysis

The most important result of this slow ramp test with a Viggen-4 fuel is the occurrence of pin failure with the low value of 810 W/cm as maximum linear power.
The rapid power shut down after failure provided valuable information on the fuel state close to failure time and on the early post-failure phenomena.

### II.4.1. Fuel pin behaviour up to failure

- Fuel melting

In opposition to the E9 and E9bis test, no hodoscope signal has been detected before pin failure to give information on power to melt.
The post-test examinations show that the molten cavity extends axially from 200 mm/BFC to 625 - 660 mm/BFC with limited radial extension :

| Axial level (mm/BFC) | Relative radial extension (% of external radius) |
|---|---|
| 220 | ~ 0 |
| 300 | 50 |
| 420 | 54 |

Due to the solid pellet design and high fuel smear density, degradation of the thermal conductivity due to fuel swelling had probably a limited effect on fuel thermal behaviour as compared with Ophelie-6 pins.

- Pin mechanical behaviour

Pin failure has been detected by the micro-phones and the hodoscope at the axial location of 60 cm (i.e. 17 cm above peak power position) and resulted in fuel ejection into liquid sodium.

At that time and location the mean clad temperature is estimated to be around 710 - 740°C.
The profilometry of the clad performed on the intact lower part of the pin has shown residual deformation of 0.6 to 1 % in the region 280 - 380 mm.
The limited radial extension of the molten fuel cavity and especially at failure location indicates that cavity pressure is not the dominant parameter to cause clad failure.

The characteristics of the high burn-up Viggen-4 fuel and the understanding of the transient fuel behaviour under more rapid power transients (TOP) in other CABRI-2 tests, led to assume that solid fuel swelling results in considerable PCMI loading of the clad.

Indeed, with such high burn-up, an important quantity of gases is retained in large bubbles at the grain boundary, in the outer zone of the fuel with grain fragmentation.
Under slow heat-up and with strong cladding constraint, the swelling of these bubbles occurs with release to free volume and leads to clad deformation.
The measurements of fission gas retention in the intact zone (EPMA and sublimation) confirm the release of such gases during the slow transient.
The axial fuel expansion is limited (2 mm given by the hodoscope) and may be explained by the fuel thermal expansion with cold outer fuel under slow power ramp.

## II.4.2. Post failure phenomena

- Fuel ejection and sodium channel voiding

At the time of pin failure, the hodoscope detected fuel ejection in the liquid sodium in the region 56 - 72 cm/BFC. This resulted in a fuel coolant interaction (FCI) as shown by inlet and outlet flow divergence (fig. 2) which reaches its maximum within 5 ms (consistent with CABRI-1 tests, [2]). Pressure peaks of 47b and 24b were respectively obtained in the lower and upper parts of the test section.

Evidence of an early fission gas release has been given by the analysis of the void detector located in the upper part of the test channel and by the response of the sodium thermocouples at the top of the fissile length and above.

Considering the pin failure conditions, these gases are assumed to be released partly from the upper plenum and from the thick solid outer fuel zone with high gas retention and possible ejection of small fuel fragments. Contribution from the solid outer fuel zone also explains the slower sodium flow decrease after divergence in comparison to CABRI-1 results with less gas quantity in the periphery.

The fuel mass ejection rate is 9 g during 50 ms and the sodium voiding is limited to the half upper part of the pin.

- *Fuel motion*

During the 150 ms between failure and scram onset the hodoscope showed only radial fuel motion with small axial relocation.

Continuous gas flow from the fuel pin is suggested by the total voiding of the molten cavity seen by the post-test examinations and by the observation of the crust on the structure wall with the dense layers and porous frozen fuel pushed inside.
The fuel relocated outside the pin created partial channel obstruction (residual sodium flow of 6 %).

No intact stub motion has been observed during the test in spite of the high plenum pressure of the Viggen-4 pins. In E12 experiment, this can be linked to the limited pin disruption which prevented from release of the cladding constraint at both ends of the pin.

The hodoscope at the final state indicates lack of fuel in the region 25- 50 cm BFC (consistent with the cavity voiding) and the post-test examinations show relocated fuel from 53 to 71 cm BFC corresponding to the ejection zone.

## III. QUANTITATIVE ANALYSIS

Quantitative evaluation of these tests have been made with the analytical models PAPAS-2S (PNC), SAS-4A-Ref. 94 (KFK) and PHYSURAC (CEA).
In the following, we will concentrate on the description of the pin behaviour up to failure.
In this frame, the interpretation of the CABRI-2 tests led to major modelling extensions due to the investigation of high burn-up fuel and lower energy injection rate compared to CABRI-1.

These improvements concern mainly :

- the description of the irradiation campaign by the way of an extended model of gap conductance in SAS-4A,

- the transient gases behaviour coupled with the pin mechanics in all the three codes.

However, although agreement is found on the basic phenomena, differences still exist in the detailed modelling.

SAS-4A describes gas release from fuel to central hole and from central hole to free volume (connected porosity , cracks). Transient fuel swelling is due to non-equilibrium bubbles growth with time constant equivalent to gas release time constant. The effect of cladding constraint is taken into account through hydrostatic fuel pressure (average between fuel-clad contact pressure and pressure in central hole).

In PAPA-2S fuel swelling is acting after grain boundary separation determined on the basis of face bubble growth and grain face tunnel formation (linkage criterion used). The release to free volume is possible after a maximum volumetric swelling of 10 %. The contact pressure between fuel and clad is assumed as hydrostatic fuel pressure.
With these assumptions, fuel swelling is closely related to the radial profile of gas retention (pre specified) and high amplitude of volumetric swelling is expected in the outer fuel zone.

In PHYSURAC, gas release to free volume and to plenum is described together with transient swelling of inter and intragranular bubbles taking into account the pressure field inside the fuel (intimate coupling with the pin mechanics). Swelling due to porosity in the internal hot part of the fuel (above softening temperature of 1800°C) is assumed with instantaneous pressure equilibrium with plenum pressure resulting in volume increase in the fuel hydrostatic zone and no gas release to plenum before central hole closure.

The degradation of the fuel thermal conductivity with the macroscopic porosity is described in SAS-4A and PHYSURAC. In PAPAS, the impact of the grain boundary separation on the thermal conductivity is simulated by a reduction factor dependant on face bubble growth down to 0.6 times the nominal value.

The fuel pin mechanics is similar in SAS-4A and PHYSURAC with fuel body separated into zones and strengthless condition based on temperature threshold.
In PAPAS, a more precise model treats the yielding behaviour of fuel and clad.

Clad mechanical properties are derived from tensile tests of the Ophelie-6 and Viggen-4 pins, with imposed strain rate in the three codes. Failure prediction is based on cladding strain in SAS-4A and PHYSURAC. Although failure prediction is possible with introduction of simple correlation for failure strain, PAPAS did not give failure prediction within this study.
In-pin fuel motion has not been considered in this study (SAS-4A model not applied).

### III.1. E9 and E9 bis calculations

In-those tests, the maximum power level at CABRI steady-state before the power ramp, is higher than the end of life maximum power, consistently with other rapid transients realized with Ophelie-6 pins.

In PHYSURAC, the whole transient starting from equivalent end-of-life conditions is described.
With PAPAS-2S, calculation usually starts from CABRI steady state condition just before transient. Although experimental correlations are available to determine the boundary condition such as restructuring and gas release for this initial state, it was specified mainly by input based on PIE information in order to reduce additional uncertainty by the boundary condition. However, for the E9 and E9bis test, the CABRI steady state operation seems to be already a kind of transient compared with the EOL conditions. Therefore, 100 seconds of pre-conditioning period in CABRI was calculated before the TOP with PAPAS-2S.

The obtained power to melt values (similar in E9 and E9 bis) are the following :

| | |
|---|---|
| SAS-4A | 763 W/cm |
| PAPAS-2S | 736 W/cm |
| PHYSURAC | 664 W/cm |

In PHYSURAC, the assumption of fuel swelling due to porosity gases in the hot part of the fuel without gas release to plenum already indicated a reduction of the inner fuel radius at CABRI-steady state level and leads probably to an under-estimation of the power to melt. However, the value is consistent with the scenario of the tests showing early fuel melting below 730 W/cm.

The slow heat-up to CABRI steady-state beyond end of life conditions has only partly contributed to the early melting onset with no influence on the final melting extension : this has been studied with PHYSURAC which showed that a slow power ramp starting directly from end of life conditions would lead to a power to melt of 730 W/cm, still lower value than 850 W/cm as originally predicted without the modelling improvements.

The figures 3, 4 and 5 show the calculated melting extension in E9 and E9 bis compared to post-test examinations. In SAS-4A, the melting extension is under-estimated with the present approach. Good agreement is found by PAPAS and PHYSURAC with however an overestimation of the axial extension in PAPAS probably linked to the low gap conductance at axial ends. The fact that satisfying results are found without description of the impact of the in-pin molten fuel relocation confirms that with regards to melting extension, its effect is not significant.

From the results, it can be concluded that the basic phenomenon to explain such low power to melt and large melting extension in the Ophelie-6 pins is the degradation of the fuel thermal conductivity due to gas release and macroscopic porosity increase during slow heat-up.
This phenomenon is strongly related to the end of life state of the Ophelie-6 pin which operated at a maximum linear power of 305 W/cm retaining thus significant amount of gases in the region of relative radius from 0.66 to 1. R/Ro.

The calculated strong gas release from solid fuel during the test is illustrated on figure 6 in agreement with the retention measurements.
The absence of plastic straining of the clad as shown by the experiment is reproduced in SAS-4A with the use of an imposed variation of the plasticity temperature fonction of contact pressure and central channel pressure.
A plastic deformation of the clad is calculated by PHYSURAC in E9, late in the transient (beyond the maximum power of 1100 W/cm) and reaches 2 %, due to high cavity pressure (32 MPa) assumed to load the clad directly. This can be explained by the underestimation of the gas release from solid fuel to plenum and by the absence of in-pile motion modelling. Similarly, cladding plasticity due to fuel thermal expansion is reached in PAPAS (0.4 % at 60 cm BFC). However further deformation due to swelling was not calculated. Without gas release to the plenum, the cavity pressure reached 60 MPa which seemed to be unrealistic and has not been transferred to the cladding due to the presence of the solid fuel shell with high strength.

### III.2. E12 calculations

The E12 calculations have been performed with the three codes using the same basic modelling as in E9 and E9 bis analysis. The differences concern in PAPAS, the absence of decrease of the fuel thermal conductivity and in SAS-4A, the use of a constant fuel plasticity temperature (2400 K).

The calculated power ramp led to power to melt of 711 W/cm (SAS-4A), 690 W/cm (PAPAS) and 638 w/cm (PHYSURAC) .The lower values given by PHYSURAC results from already hotter fuel temperature at CABRI-steady-state (200 °K in the center) due to the calculated effect of porosity increase and swelling in central hole from end-of-life equivalent conditions.

The figures 7 and 8 represent the melting extension compared to post-test examinations and corresponding to the maximum power of 810 W/cm at failure time.
A good agreemeent is found by PHYSURAC and SAS-4A. This confirms, that even with solid fuel, degradation of the thermal conductivity due to fuel porosity increase, although lower than with hollow pellets may better explain the results.

The transient calculations did not lead to precise description of the pin failure except in PAPAS in which a maximum clad deformation of 3 % leading to failure has been obtained consistently with the experiment at the level 60 cm. At this level similar maximum clad temperature is calculated (710 - 740 °C) by all codes.
The axial profile of clad plastic deformation (figure 9) shows that in SAS-4A the maximum value (1 %) is found at PPN while in PHYSURAC and PAPAS, the zone of maximum deformation is 50-60 cm which can be correlated to the axial profile of initial gas retention and cladding temperature.

The high straining found in PAPAS results mainly from the assumptions of high level gas retention in the radial zone from 0.75 to 1. in relative radius, possible high volumetric swelling up to 10 % without gas release and fuel mechanical modelling with hydrostatic pressure given by contact pressure between fuel and clad (assumption linked to the high level of grain fragmentation in the periphery of the VIGGEN-4 fuel).
On the other hand, the insufficient plastic clad deformation calculated by PHYSURAC at 60 cm may be explained by the limitation of the fuel swelling in the outer zone of the fuel due to the assumption of elastic fuel behaviour below 1800 °C giving high stress field.

At experimental failure time, the calculated massic fuel melt fraction is 10 % with however almost liquidus fuel in cavity to be ejected.
The pin failure conditions obtained with limited melting at failure site, the deformation observed in the lower part and the analytical results confirmed the role of solid fuel swelling due to fission gases on the clad loading.
However, the contribution of the vaporisation of the cesium on the clad deformation, although difficult to evidence, has also to be considered in such slow transients with high burn-up pins.

The results given by the different codes confirmed the importance of the description of the gases behaviour (after irradiation and during the transient) coupled with appropriate mechanical fuel evolution.
Due to the present uncertainty on these points in the field of high burn-up, the description of the pin behaviour cannot be expected with high level of precision.

## IV. CONCLUSION

The analysis of the CABRI-2 slow ramp tests has evidenced the major role of fission gases during the whole transient and the different fuel pin behaviours of hollow and solid pellet design.

In the case of the hollow pellets of Ophelie-6 fuel with medium burn-up and low smear density reduced by clad swelling, large fuel swelling resulted in degradation of the fuel conductivity and led to a rather hot fuel state with low power to melt.
On the other hand, the absence of clad deformation and consequently of failure, in both tests E9 and E9bis confirmed the high margin to deterministic pin failure (above 1350 W/cm) under the CABRI neutronic flux conditions. Such a behaviour is explained by the low smear density and the reduction of the cavity pressure due to in-pin motion and outgassing from the molten fuel.

With the solid pellet design of Viggen-4 pins and high burn-up level of 12 at %, the solid fuel swelling due to fission gases retained in the outer fuel zone with high grain fragmentation, resulted in clad deformation and failure at the maximum linear heat rate of 810 W/cm. Possible contribution of volatile fission products has also to be considered.

The pin failure led to fuel ejection with a massic molten fuel fraction of only 10 %, which initiated FCI and led to partial channel obstruction.
However, such post-failure behaviour and consequences on propagation inside a subassembly cannot be directly extrapolated to the case of an adventitious failure of a fuel pin with an hollow pellet design and 10 % melt fraction due to the different cavity conditions and especially cavity pressure for fuel ejection, the different coolant channel geometry and the rapid power shut down after failure.

Although these CABRI-2 slow ramp tests are not fully prototypic of the reactor case due to the radial flux depression in the CABRI-core, they have clearly underlined that the fuel performance under such transients is mainly influenced by gas and fission products retention.
High burn-up level or low power operating conditions leads to increase the probability of early pin failure with solid pellet design and to a reduction of the power to melt in case of hollow pellet design.

However, the failure level with hollow pellet fuel design increases considerably when compared to the solid pellet fuel pin design.

To represent such behaviours in computer codes as PHYSURAC, PAPAS-2S and SAS-4A REF94, major extensions of the physical modelling were necessary. However, the difficulties encountered to get precise description of the phenomena showed the need of more refined pin mechanics modelling coupled with transient fission gases behaviour and in-pin fuel motion.

## REFERENCES

[1] M. HAESSLER and all.
*"The CABRI-2 Programme - Overview on results."*
Vol II, p. 209, International Fast Reactor Safety Meeting, SNOWBIRD, August 1990

[2] M. CRANGA and all.
*"Transient material behaviour in CABRI-1 experiment failure under fully and semi-restrained fuel pin conditions."*
Vol.I, p. 421International Fast Reactor Safety Meeting, SNOWBIRD, August 1990

[3] D. STRUWE and all.
*"Two-phase flow, clad melting and transient materials relocation in the CABRI-1 experiments".*
Vol I, p. 431, International Fast Reactor Safety Meeting, SNOWBIRD, August 1990

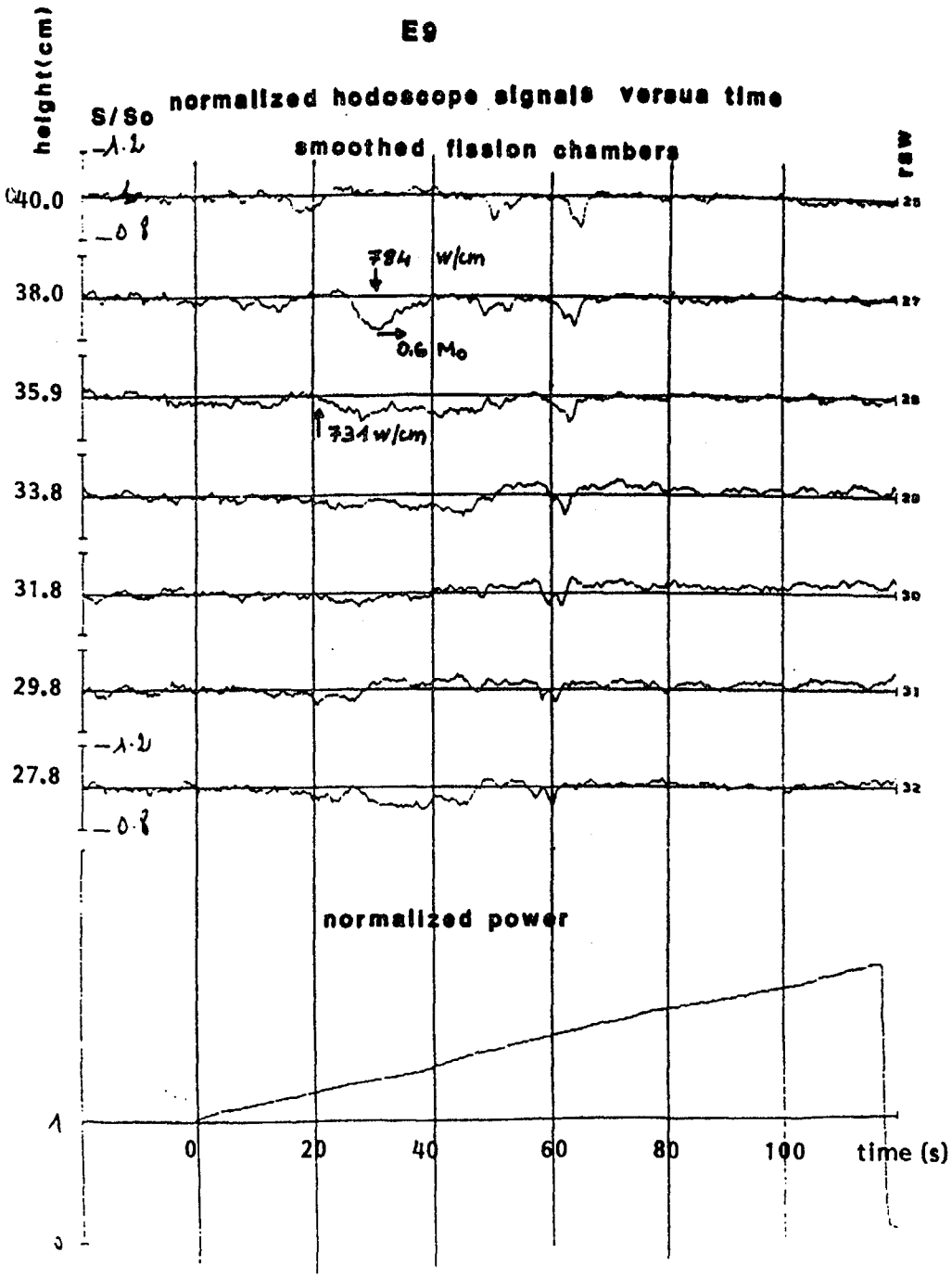
E9
normalized hodoscope signals versus time
S/So
smoothed fission chambers
height(cm)
raw
40.0
38.0
35.9
33.8
31.8
29.8
27.8
784 w/cm
0.6 Mo
731 w/cm
normalized power
1
0
0
20
40
60
80
100
time (s)

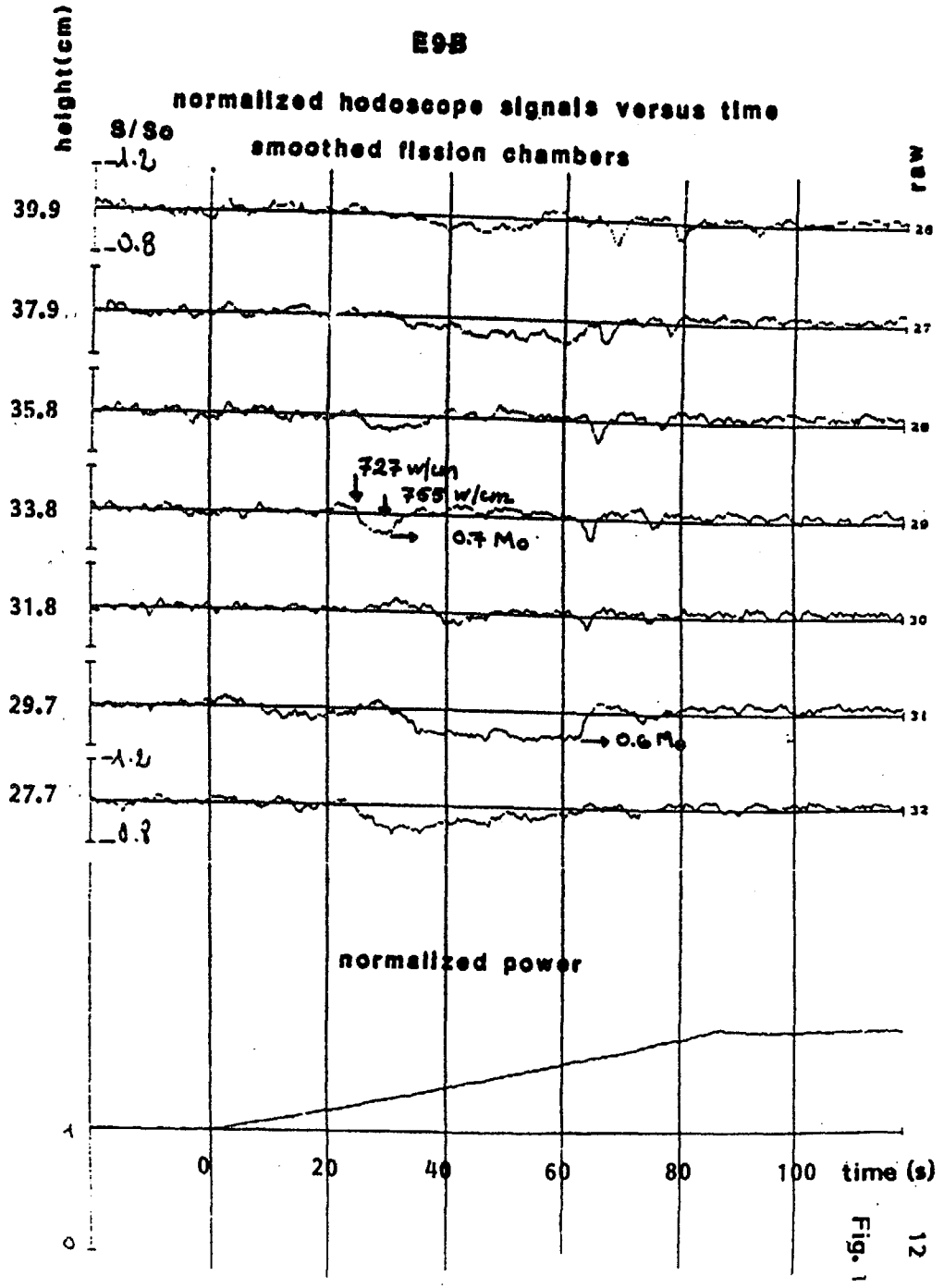
E9B
normalized hodoscope signals versus time
S/So
smoothed fission chambers
height(cm)
raw
39.9
37.9
35.8
33.8
31.8
29.7
27.7
727 w/cm
765 w/cm
0.7 Mo
0.6 Mo
normalized power
1
0
0
20
40
60
80
100
time (s)

Fig. 12

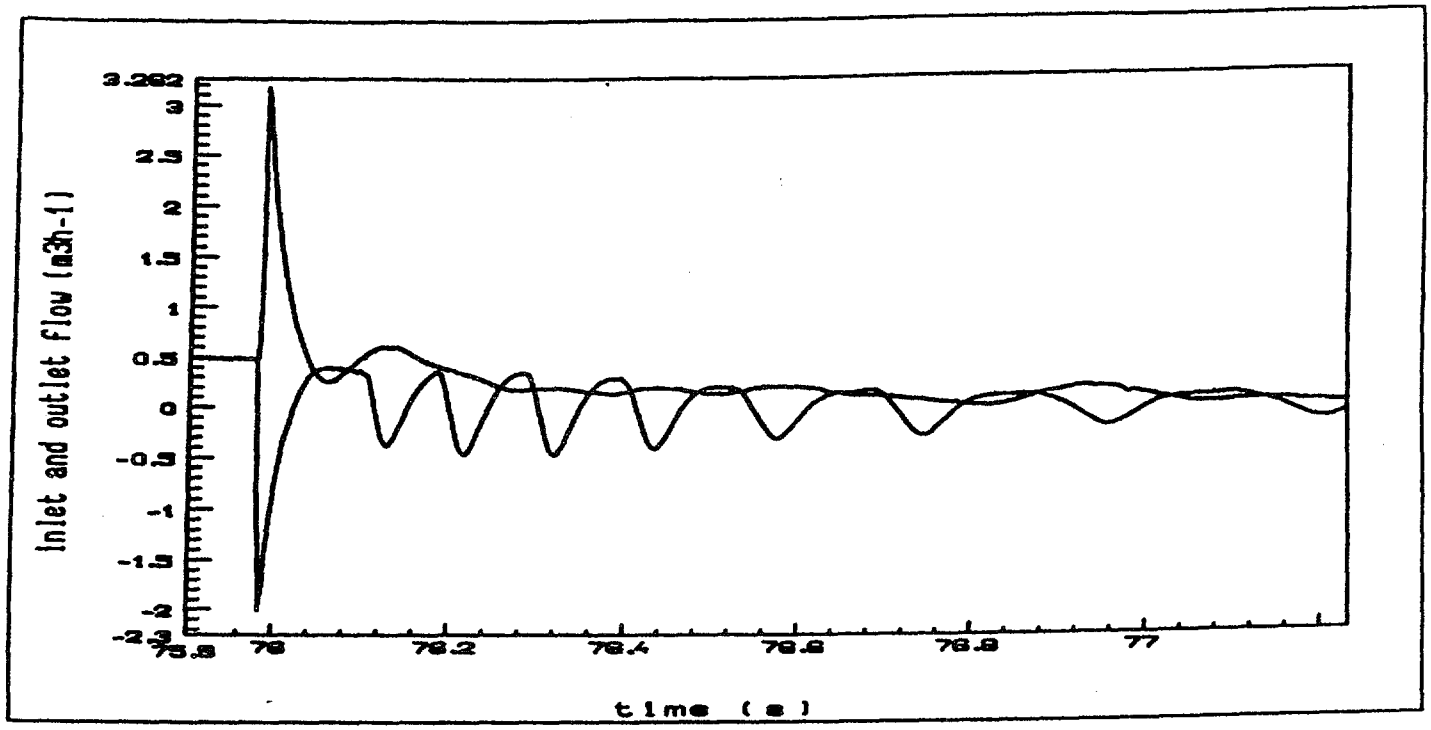


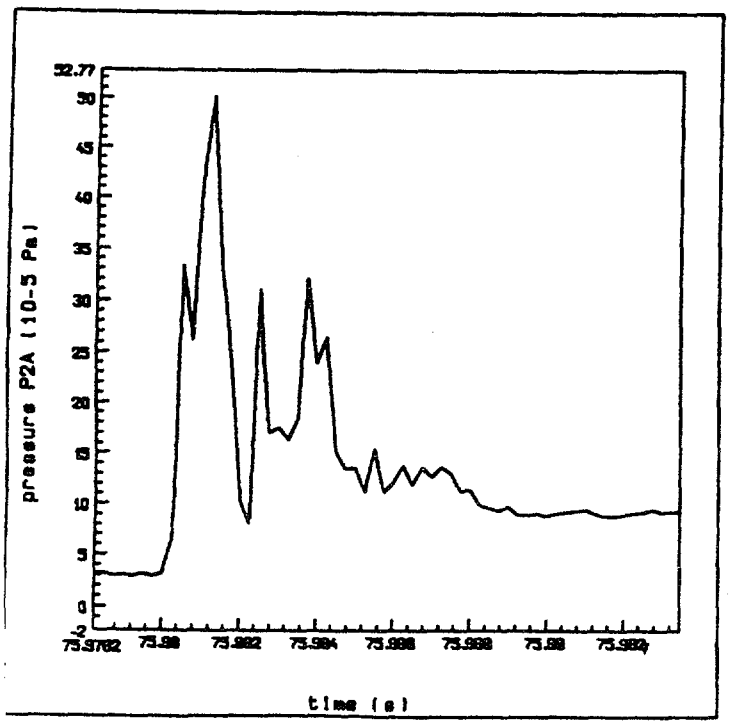


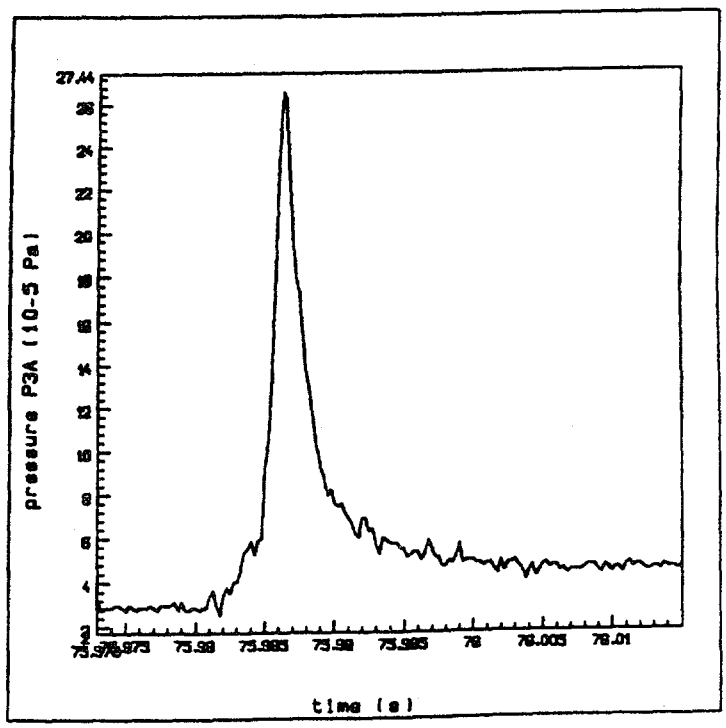


Fig.2 E12 post failure events

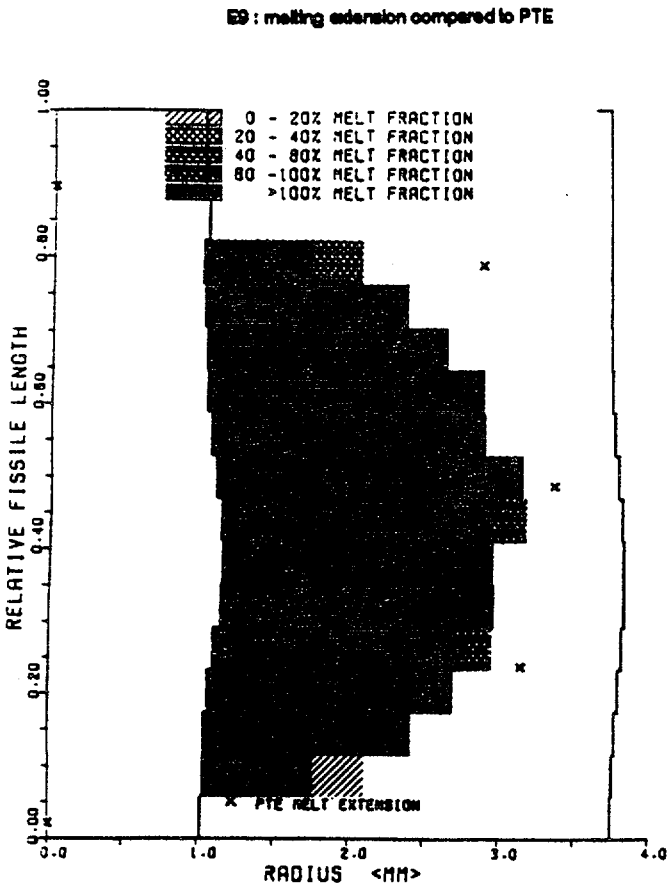


Fig. 3 : SA94A

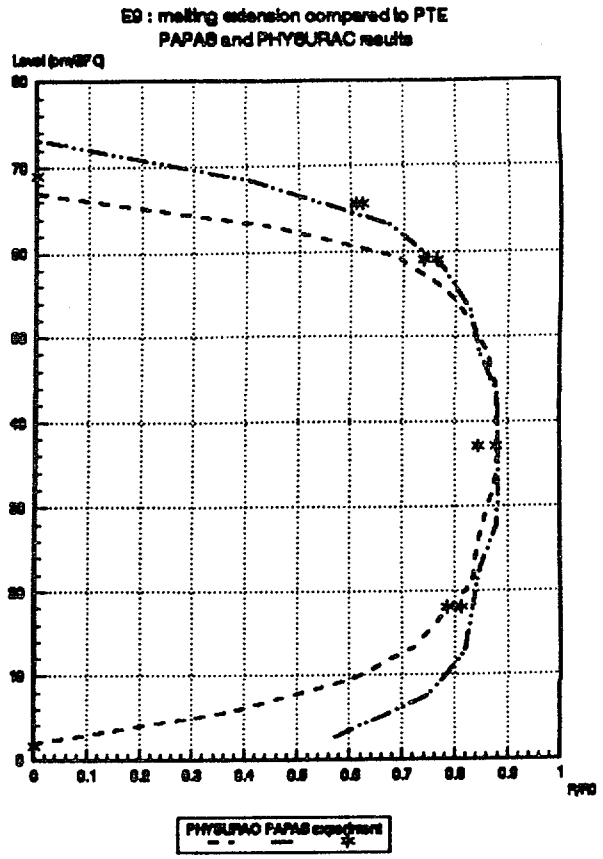


Fig. 4

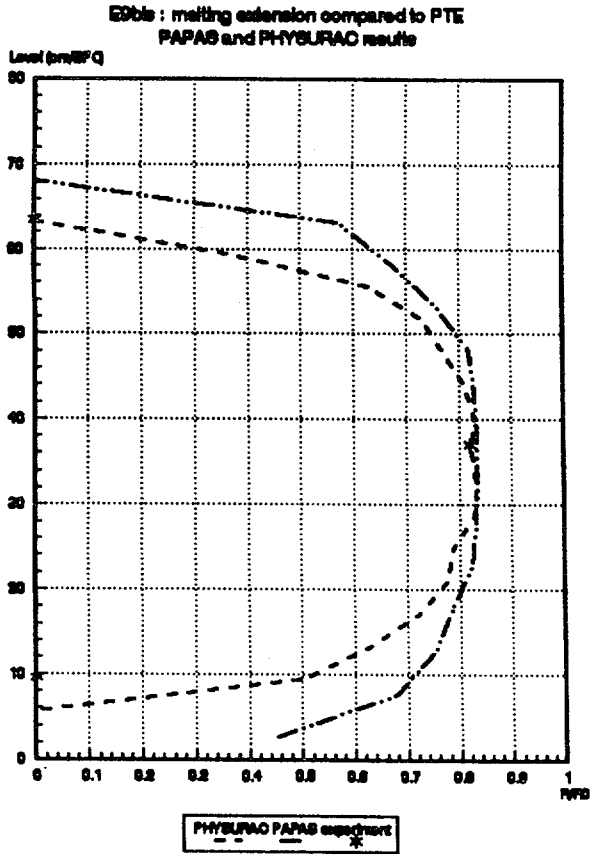


Fig. 5

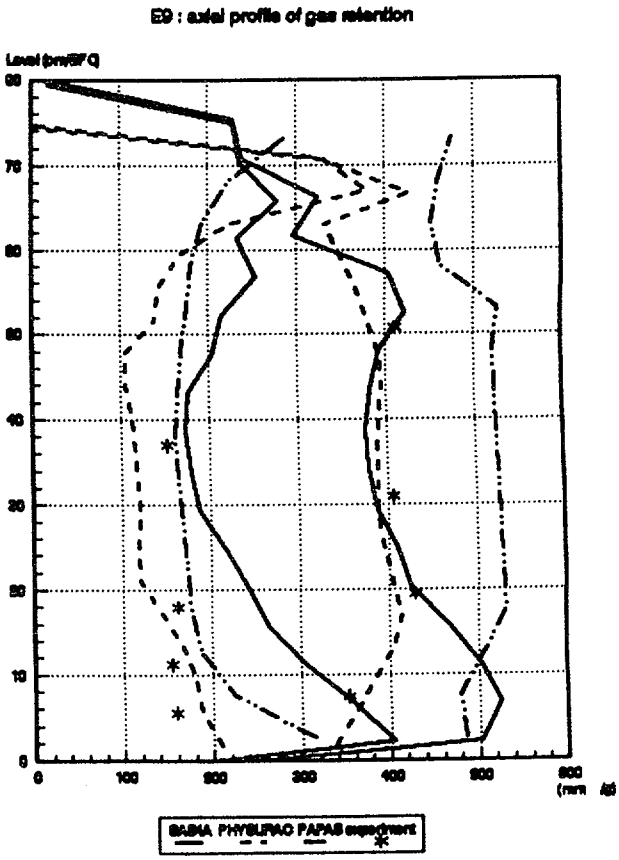


Fig. 6

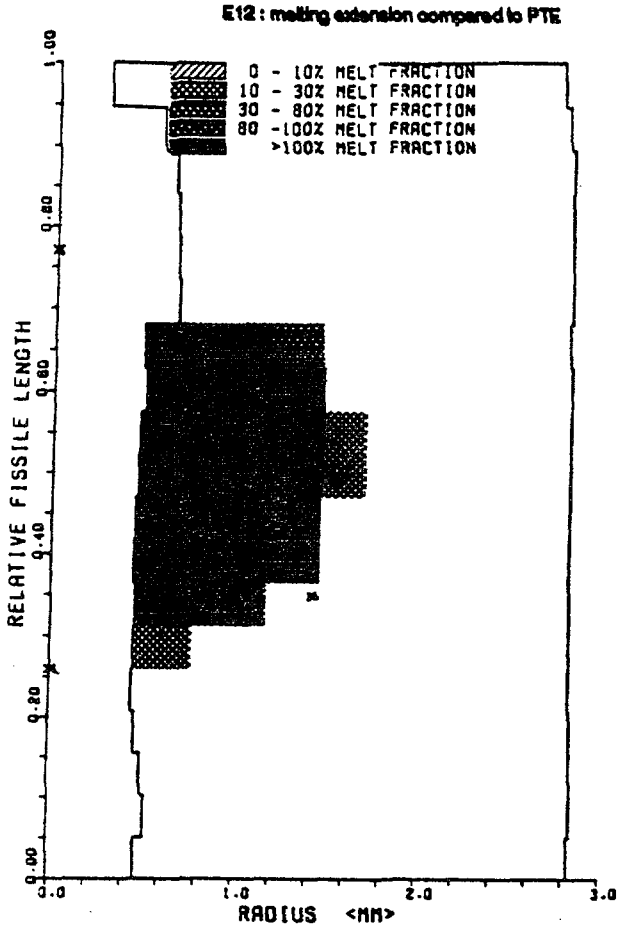


Fig. 7 : SAS4A

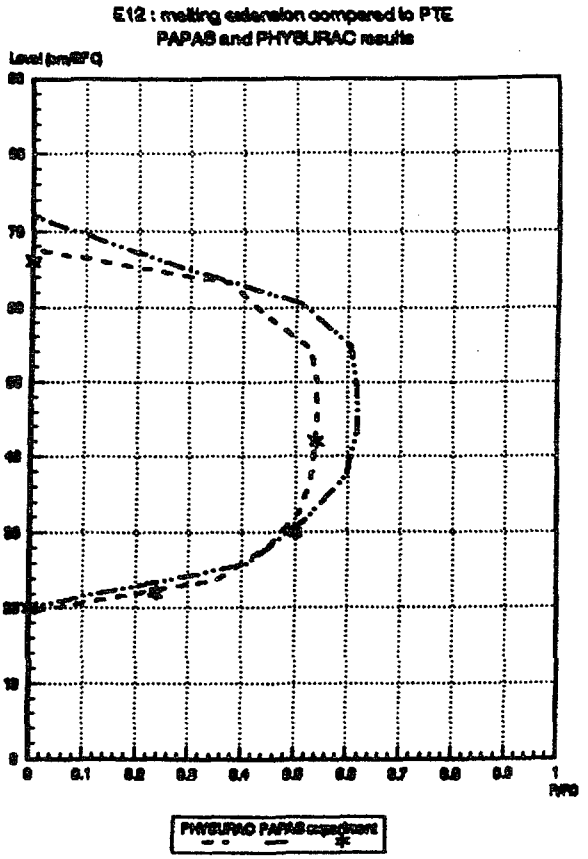


Fig. 8

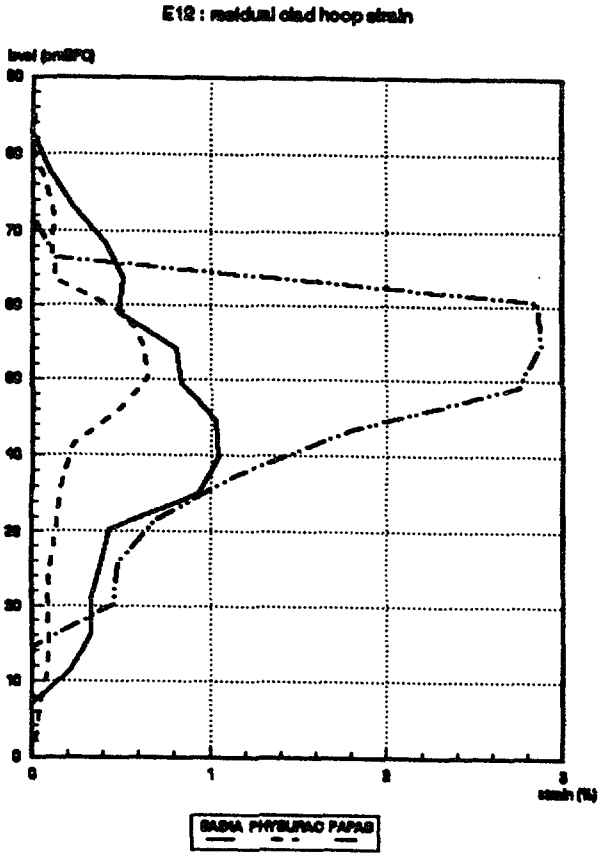


Fig. 9